Medical Engineering and Physics 76 (2020) 47–55

Contents lists available at ScienceDirect

Medical Engineering and Physics

journal homepage: www.elsevier.com/locate/medengphy

Strain stiffening of peripheral nerves subjected to longitudinal extensions in vitro

Elisabetta Giannessi[a,1], Maria Rita Stornelli[a], Pier Nicola Sergi[b,1,*]

[a] Department of Veterinary Science, University of Pisa, 56124 Pisa, Italy
[b] Translational Neural Engineering Area, The Biorobotics Institute, Sant'Anna School of Advanced Studies, PSV, 56025 Pontedera, Italy

ARTICLE INFO

Article history:
Received 20 June 2018
Revised 11 October 2019
Accepted 20 October 2019

Keywords:
Strain stiffening
Peripheral nerves
Tangent modulus
Instantaneous stiffness
Neuromalacia
Pathological nerve softening

ABSTRACT

The mechanical response of peripheral nerves is crucial to understand their physiological and pathological conditions. However, their response to external mechanical solicitations is still partially unclear, since peripheral nerves could behave in a quite complex way. In particular, nerves react to longitudinal strains increasing their stiffness to keep axons integrity and to preserve endoneural structures from overstretch. In this work, the strain stiffening of peripheral nerves was investigated in vitro through a recently introduced computational framework, which is able to theoretically reproduce the experimental behaviour of excised tibial and sciatic nerves. The evolution and the variation of the tangent modulus of tibial and sciatic nerve specimens were quantitatively investigated and compared to explore how stretched peripheral nerves change their instantaneous stiffness.

1. Introduction

Nerve impulses travel up peripheral nerves [45,48] to the central nervous system, connecting the brain to the periphery of the body. Peripheral nerves differently react to external mechanical stimuli, according to their state of health. A deep knowledge of their mechanical response is, therefore, required to recognise physiological and pathological conditions, as well as to avoid damages due to excessive mechanical solicitations. Indeed, healthy nerves can withstand mechanical loads and increase their length to accomplish the movement of joints [48]. However, in pathological conditions (i.e., neuromalacia) peripheral nerves apparently keep their structural integrity, but lose their stiffness. This pathological softening was described by Johnson and Storts [21] in animals (e.g.,chickens,birds) exposed to a diet highly deficient in riboflavin (vitamin B12). Similarly, Nonaka et al. [34] described neuromalacia in human beings, as an adverse effect of particular medical treatments (i.e., radiations). Millesi et al. [31] found that large cyclic or suddenly mechanical solicitations (e.g., stretch, compression) can damage the internal structure of healthy nerves, leading to reversible or even irreversible neuropathies [26]. In a similar way, Main et al. [29] found that the compression of median nerve may result in the carpal tunnel syndrome, while Williams et al. [52] described how the looping of the laryngeal nerve around the aortic arch could led to the unilateral vocal fold paralysis. Finally, Castro and Frank [4], as well as Greenberg et al. [16], reported that the overstretch of healthy stiff nerves in arms and legs could led to the "stinger syndrome".

Furthermore, the knowledge of the mechanical response of nerves is strategic in novel emerging scientific fields (e.g., neuroengineering), involving the connection between nerve tissue and artificial devices. To this aim, Ma et al. [28] studied the in vivo and in vitro mechanical response of nerves to asses intraoperative conditions, while the interactions between peripheral nerves and tungsten microneedles [39,40,54] were investigated to optimize the insertion of intraneural interfaces [6,37].

As a consequence, in this work a theoretical framework is provided to investigate the evolution of the instantaneous stiffness of peripheral nerves subjected longitudinal strain, since it is crucial in early identification of nerve disfunctions, as well as strategic to better design the connection between nerves and biomaterials, avoiding tissue scarring formation due to stiffness mismatch [25].

2. Materials and methods

2.1. Experiments

Each specimen was dissected from a tibial nerve of an adult pig and frozen ($\simeq -18\,^{\circ}C$) until experiments. The length and the cross sectional area of the frozen specimens were measured through a

* Corresponding author.
E-mail address: p.sergi@sssup.it (P.N. Sergi).
[1] Both authors contributed equally to this work.

https://doi.org/10.1016/j.medengphy.2019.10.012
1350-4533/

graded aluminium scale and resulted in 82 mm and 26.073 mm^2. Experiments were performed at room temperature ($\simeq 25^\circ$), using an Instron R4464 testing machine (Instron Corporation, Canton, MA) equipped with a standard load cell (Instron load cellâInstron Corporationâcell type 2525 – 808, max force 10 N, accuracy in the range 0–1% Full Scale Output). The specimen was fixed to the testing machine through custom clamps, so the length between clamps was 70 mm. The mechanical characteristics of the nerve were preserved by regularly spraying saline on its external surface, while its viscous response was stabilized through a preconditioning procedure [11]. The specimen was, therefore, stretched up to 8% to shortly overcome its physiological limits. Finally, a quantitative comparison between the mechanical response of a tibial and a sciatic nerves was provided [14].

2.2. Theoretical framework

Peripheral nerves were modelled as a homogeneous and incompressible material, ruled by the following hyperelastic polynomial strain energy function [13,53]:

$$\Psi(I_1) = \sum_{i=1}^{3} c_i (I_1 - 3)^i \tag{1}$$

where c_1, c_2, $c_3 \in \Re$ were scalar coefficients. The first strain invariant (I_1) and the deformation gradient **F** were used to write the Cauchy stress as:

$$\sigma = -k\mathbf{I} + 2\frac{\partial \Psi(I_1)}{\partial I_1}\mathbf{F}\mathbf{F}^{\mathbf{T}} \tag{2}$$

where k was an indeterminate Lagrange multiplier related to boundary conditions, while **I** and $\mathbf{F}^{\mathbf{T}}$ were, respectively, the unit tensor and the transposed deformation gradient. Since $I_1 = tr(\mathbf{F}\mathbf{F}^{\mathbf{T}})$ and **F** were expressed as a function of principal stretches, Eq. (2) was able to provide a theoretical relationship between stress and stretch.

A homogeneous triaxial stretch state was assumed and the k coefficient was computed, accounting for the material incompressibility together with the experimental boundary conditions. Then, the longitudinal component of the Cauchy stress was expressed as:

$$\sigma_z(\lambda, c_1, c_2, c_3) = \frac{2(\lambda - 1)(\lambda^2 + \lambda + 1) f(\lambda, c_1, c_2, c_3)}{\lambda^3} \tag{3}$$

where $f(\lambda) = 3c_3\lambda^6 + (2c_2 - 18c_3)\lambda^4 + 12c_3\lambda^3 + (27c_3 - 6c_2 + c_1)\lambda^2 + \lambda(4c_2 - 36c_3) + 12c_3$.

The mean Cauchy stress was written as a function of strain as:

$$\sigma_z(\epsilon, c_1, c_2, c_3) = \frac{Q(\epsilon, c_1, c_2, c_3)}{\epsilon^3 + 3\epsilon^2 + 3\epsilon + 1} \tag{4}$$

where $Q(\epsilon, c_1, c_2, c_3) = 6c_3\epsilon^9 + 54c_3\epsilon^8 + (180c_3 + 4c_2)\epsilon^7 + (270c_3 + 28c_2)\epsilon^6 + (162c_3 + 72c_2 + 2c_1)\epsilon^5 + (84c_2 + 10c_1)\epsilon^4 + (36c_2 + 20c_1)\epsilon^3 + 18c_1\epsilon^2 + 6c_1\epsilon$.

Similarly, the tangent modulus ($E_t = d\sigma/d\epsilon$) was written as:

$$E_t(\epsilon, c_1, c_2, c_3) = \frac{G(\epsilon, c_1, c_2, c_3)}{\epsilon^4 + 4\epsilon^3 + 6\epsilon^2 + 4\epsilon + 1} \tag{5}$$

where $G(\epsilon, c_1, c_2, c_3) = 36c_3\epsilon^9 + 324c_3\epsilon^8 + (1152c_3 + 16c_2)\epsilon^7 + (2070c_3 + 112c_2)\epsilon^6 + (1944c_3 + 312c_2 + 4c_1)\epsilon^5 + (810c_3 + 444c_2 + 20c_1)\epsilon^4 + (336c_2 + 40c_1)\epsilon^3 + (108c_2 + 42c_1)\epsilon^2 + 24c_1\epsilon + 6c_1$, while the rate of change of the tangent modulus with strain ($E_t' = dE_t/d\epsilon$) was expressed as:

$$E_t'(\epsilon, c_1, c_2, c_3) = \frac{M_1(\epsilon, c_1, c_2, c_3)}{\epsilon^4 + 4\epsilon^3 + 6\epsilon^2 + 4\epsilon + 1} - \frac{M_2(\epsilon, c_1, c_2, c_3)}{\left(\epsilon^4 + 4\epsilon^3 + 6\epsilon^2 + 4\epsilon + 1\right)^2} \tag{6}$$

where $M_1(\epsilon, c_1, c_2, c_3) = 324c_3\epsilon^8 + 2592c_3\epsilon^7 + 7(1152c_3 + 16c_2)\epsilon^6 + 6(2070c_3 + 112c_2)\epsilon^5 + 5(1944c_3 + 312c_2 + 4c_1)\epsilon^4 + 4(810c_3 + 444c_2 + 20c_1)\epsilon^3 + 3(336c_2 + 40c_1)\epsilon^2 + 2(108c_2 + 42c_1)\epsilon + 24c_1$, and $M_2(\epsilon, c_1, c_2, c_3) = (4\epsilon^3 + 12\epsilon^2 + 12\epsilon + 4)[36c_3\epsilon^9 + 324c_3\epsilon^8 + (1152c_3 + 16c_2)\epsilon^7 + (2070c_3 + 112c_2)\epsilon^6 + (1944c_3 + 312c_2 + 4c_1)\epsilon^5 + (810c_3 + 444c_2 + 20c_1)\epsilon^4 + (336c_2 + 40c_1)\epsilon^3 + (108c_2 + 42c_1)\epsilon^2 + 24c_1\epsilon + 6c_1]$.

2.3. Identification of parameters

The optimum values for numerical coefficients in Eq. (3) were found through a non-linear procedure (quasi-Newton algorithm, Scilab © Scilab Enterprises S.A.S 2015), allowing the R^2 statistic to be maximized. More specifically, guess values of [c_1, c_2] were chosen, while c_3 was varied within a suitable range. Therefore, once computed the optimum value of c_3, the best guess of c_2 was found. Finally, once fixed the optimum values of c_2 and c_3, the best guess of c_1 was found. Furthermore, to investigate the sensitiveness of the best fitting curve to each coefficient, a quantitative index was defined as follows:

$$S(\Delta C_i) = \frac{\int_1^{\lambda_{max}} |\sigma(\lambda, C_{i^*}) - \sigma(\lambda, C_{i^*} + \Delta C_i)| d\lambda}{\Delta C_i} \tag{7}$$

where C_{i^*} were related to the best fitting curve, ΔC_i were the differences between the actual value of c_i and the target values C_{i^*}, while λ_{max} was the maximum stretch. In particular, coefficients c_i were varied to investigate the influence of these changes on the global output.

3. Results

Theoretical predictions were compared to experiments in order to assess the suitability of the provided framework in reproducing the mean Cauchy stress for an axially stretched tibial nerve. Both experimental data (squares) and theoretical predictions (solid line) evolved in a non linear way, as shown in (Fig. 1(a)). More specifically, residuals between experimental and predicted stress were within −0.1 kPa up to $\lambda = 1.05$, while oscillation between 0.25 kPa and −0.3 kPa were found for $1.05 < \lambda < 1.08$. Numerical parameters, which allowed Eq. (3) to closely reproduce experiments ($R^2 \simeq 0.992$), were $c_1 = 0.024$ kPa, $c_2 = 0.579$ kPa, $c_3 = 7.730$ MPa, as shown in Figure 1(c) (logarithmic scale).

Similarly, theoretical predictions were compared to experiments also for a sciatic nerve (Fig. 2(a)). In this case, residual differences were within 0.1 kPa up to $\lambda = 1.06$, while they oscillated between −0.2 kPa and 0.2 kPa for $1.06 < \lambda < 1.08$. In addition, Eq. (3) was able to closely reproduce experiments ($R^2 = 0.996$) for $c_1 = 3.000$ kPa, $c_2 = 3.118$ kPa, $c_3 = 3.775$ MPa, as shown in Figure 2(c) (logarithmic scale).

A further investigation was performed to explore the effect of the variation of parameters c_1, c_2, c_3 had on the evolution of Eq. (3) for the tibial nerve specimen. In particular, the slope of the stress curve varied proportionally to the variation of the c_1 parameter (i.e., $\Delta C_1 = 0.1, 0.5, 1, 10, 100, 1000$). Similarly, the effects on the theoretical stress predictions due to the variation of c_2 (i.e., $\Delta C_2 = 0.1, 0.5, 1, 10, 100, 1000$) and c_3 (i.e., $\Delta C_3 = 0.1, 0.5, 1, 10, 100, 1000$) parameters were described respectively in Figure 3(b) and (c). In both cases, the stress curve evolved in a non linear way, even if the effects of ΔC_2 overcame the influence of ΔC_3. Finally, the sensitiveness index (SI) was calculated for each coefficient, and resulted in $SI_{c_1} = 1.921 \cdot 10^{-2}$, $SI_{c_2} = 3.544 \cdot 10^{-4}$, $SI_{c_3} = 6.500 \cdot 10^{-6}$, as shown in Figure 3(d).

Furthermore, the effects the variation of parameters c_1, c_2, c_3 had on the evolution of Eq. (3) for the sciatic nerve specimen were investigated. More specifically, the more the c_1 parameter increased (i.e., $\Delta C_1 = 0.1, 0.5, 1, 10, 100, 1000$), the more the shape

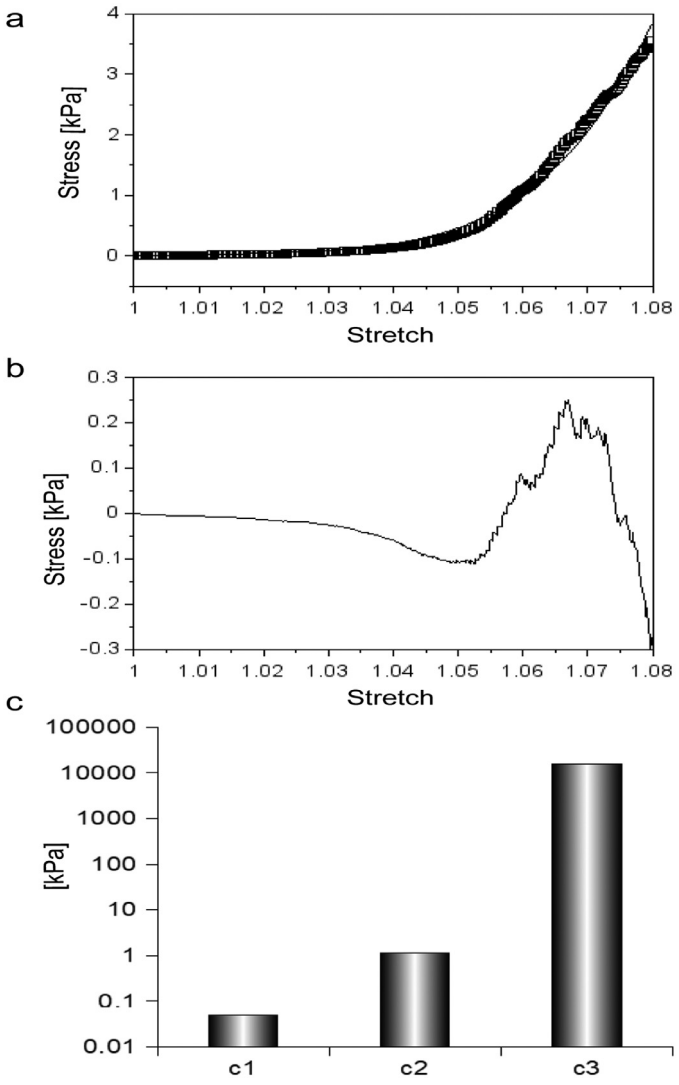

Fig. 1. (a) Comparison between experimental data (squares) and theoretical predictions (solid line) for a tibial nerve specimen. (b) Residual difference between theoretical predictions and experimental data. (c) Values of numerical parameters c_1, c_2, c_3 (logarithmic scale).

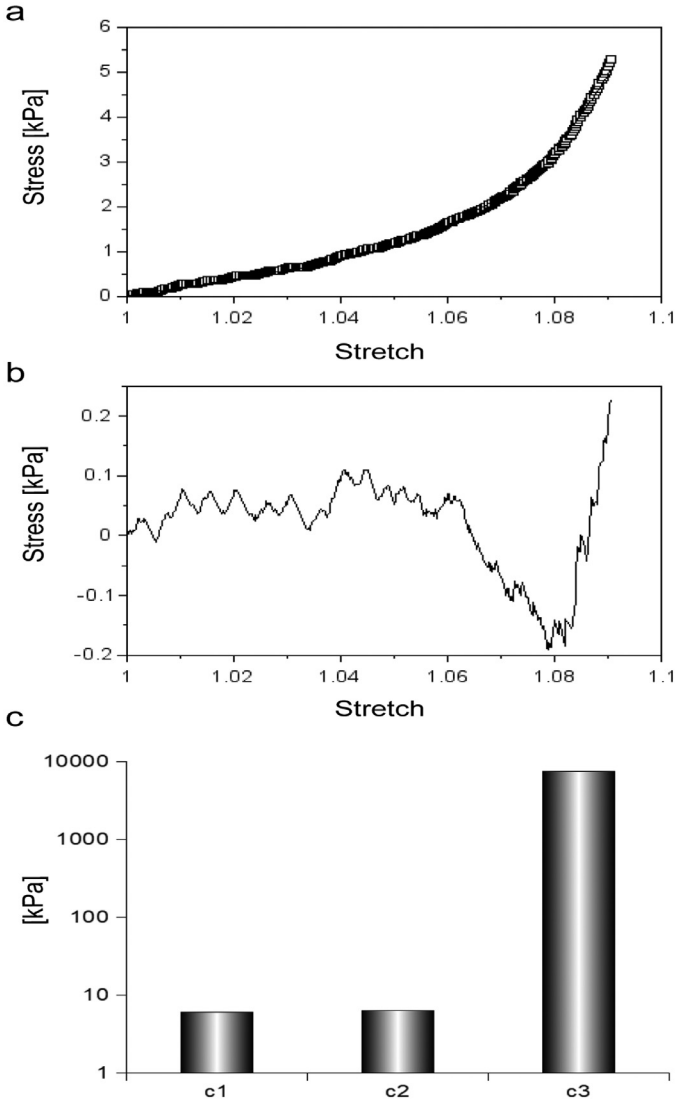

Fig. 2. (a) Comparison between experimental data (squares) and theoretical predictions for a sciatic nerve specimen (solid line). (b) Residual difference between theoretical predictions and experimental data. (c) Values of numerical parameters c_1, c_2, c_3 (logarithmic scale).

of the stress curve approached a straight line. In the same way, the variation of parameters c_2 (i.e., $\Delta C_2 = 0.1, 0.5, 1, 10, 100, 1000$), c_3 ($\Delta C_3 = 0.1, 0.5, 1, 10, 100, 1000$) resulted in changes of the stress curve shape, as shown in Fig. 4(b) and (c). Finally, the sensitiveness index was computed (see Fig. 4(d)) for all coefficients c_1, c_2, c_3, resulting in $SI_{c_1} = 1.921 \cdot 10^{-2}$, $SI_{c_2} = 3.544 \cdot 10^{-4}$, $SI_{c_3} = 6.500 \cdot 10^{-6}$.

The evolution of the stress-strain curve was then studied for both tibial and sciatic nerve specimens (Fig. 5). The increase of the mean Cauchy stress in the sciatic nerve (dashed line) exceeded that in the tibial nerve (solid line) for $0 \leq \epsilon \leq 0.07$. On the contrary, the stress within the tibial nerve exceeded that in the sciatic nerve for $0.07 \leq \epsilon \leq 0.08$ (Fig. 5(a)). In addition, the mean stress values were the same for both specimens at $\epsilon = 0$ and at $\epsilon = 0.075$. As a consequence, the difference between these stress functions had a stationary point at $\epsilon = 0.0499$, which was a point of minimum (Fig. 5(b)). Finally, the ratio between stress in tibial and sciatic nerves was found to range between 0.008 and 1.750, respectively at $\epsilon \simeq 0$ and at $\epsilon = 0.08$, as shown in Figure 5(c).

To investigate how numerical constants in Eq. (3) varied between each other, their differences were computed for both nerves. More specifically, they resulted in $|c_1 - c_2| = 0.555$ kPa, $|c_1 - c_3| = 7.730$ MPa, $|c_2 - c_3| = 7.729$ MPa, and $|c_1 - c_2| = 0.118$ kPa, $|c_1 - c_3| = 3.741$ MPa, $|c_2 - c_3| = 3.741$ MPa, respectively for the tibial and sciatic nerves (Fig. 6(a) in logarithmic scale). In addition, the intra specimens variability of each constant resulted in $\Delta c_1 = 2.975$ kPa, $\Delta c_2 = 2.539$ kPa, $\Delta c_3 = 3.985$ MPa (Fig. 6(b) in logarithmic scale). Finally, the amount of work (for a unit of volume) needed to stretch the specimens up to $\epsilon = 0.08$ resulted in 0.051 J and 0.083 J, for the tibial and sciatic nerve specimens, respectively (Fig. 6(c)).

The evolution of the tangent modulus was therefore studied for both specimens (Fig. 7). In particular, the tangent modulus of the tibial nerve ranged between 0.145 kPa and 228.454 kPa (solid line), while the tangent modulus of the sciatic nerve ranged between 18.000 kPa 130.536 kPa (dashed line). In addition, from a side, the tangent modulus of the sciatic nerve exceeded that in the tibial nerve for small strain. From the other side, the tangent modulus of the tibial nerve exceeded that in the sciatic nerve for large strain. As a consequence, both moduli had the same value at $\epsilon = 0.0499$ (Fig. 7(b)), while, for $0 \leq \epsilon \leq 0.08$, their difference ranged between -17.861 kPa and 97.917 kPa. Finally, the ratio between these moduli was explored. This ratio ranged between 0.008 and 1.750 (Fig. 7(c)), increased in a slow way for $0 < \epsilon \leq 0.015$, while its

slope was almost constant for $0.03 < \epsilon < 0.06$. On the contrary, it slowly decreased for $0.07 < \epsilon \leq 0.08$.

Similarly, the rate of change of the tangent modulus (E_t') was investigated. E_t' ranged between 0 kPa and 11096.398 kPa for the tibial nerve specimen (solid line), while it varied between 0 kPa and 5422.2339 kPa (dashed line) for the sciatic nerve specimen (Fig. 8(a)). In addition, the difference between these two rates ranged from 0 to 5674.1631 kPa (Fig. 8(b)). Finally, the ratio between rates ranged from 0.177 to 2.046 kPa, showing a fast increase for $0 < \epsilon \leq 0.02$, while for $0.04 \leq \epsilon \leq 0.08$ the slope of this curve was small (Fig. 8(c)).

4. Discussion

Peripheral nerves are stiff enough to withstand longitudinal solicitations and stretchable enough to follow the movements of joints [9,10]. Several studies have attempted to assess their limit stretch, resulting in irreversible histologic and functional changes. However, quite different results were found in experiments involving different animal models. Indeed, Highet and Sanders [20] reported that the popliteal nerve of dog was undamaged when its structure was elongated of 6%, while for an elongation of 11% the structural damages were globally severe. On the contrary, Denny-Brown et al. [8] described that peroneal nerves were functionally undamaged for elongations of about 100%. Again, Vogl et al. [49] discovered that in rorqual whales, tongue and ventral grooved blubber nerves were able to withstand extreme elongations within their physiological range. As a consequence, for our animal model (pig), no evident structural damages were expected because of the small and physiological strain range used in experiments (see also [13] for a similar strain range, and Bora et al. [3] and Grewal et al. [17] for experiments involving larger extensions). Nevertheless, in other cases, the maximum strain limit should be carefully considered in order to avoid internal damages. Indeed, Highet and Holmes [19] assessed that the maximum safe stretch for human beings to close gap and to suture a severed nerve without grafting was 9 cm (whose 25% was believed to be the true elongation and 75% was caused by the mobile nerve straightening), while Terzis et al. [47] assessed that the maximum safe axial extension of a sutured nerve was 4 times of its diameter.

Although it is well known that “the mechanical properties of the nerve maintain the integrity and function of its components”

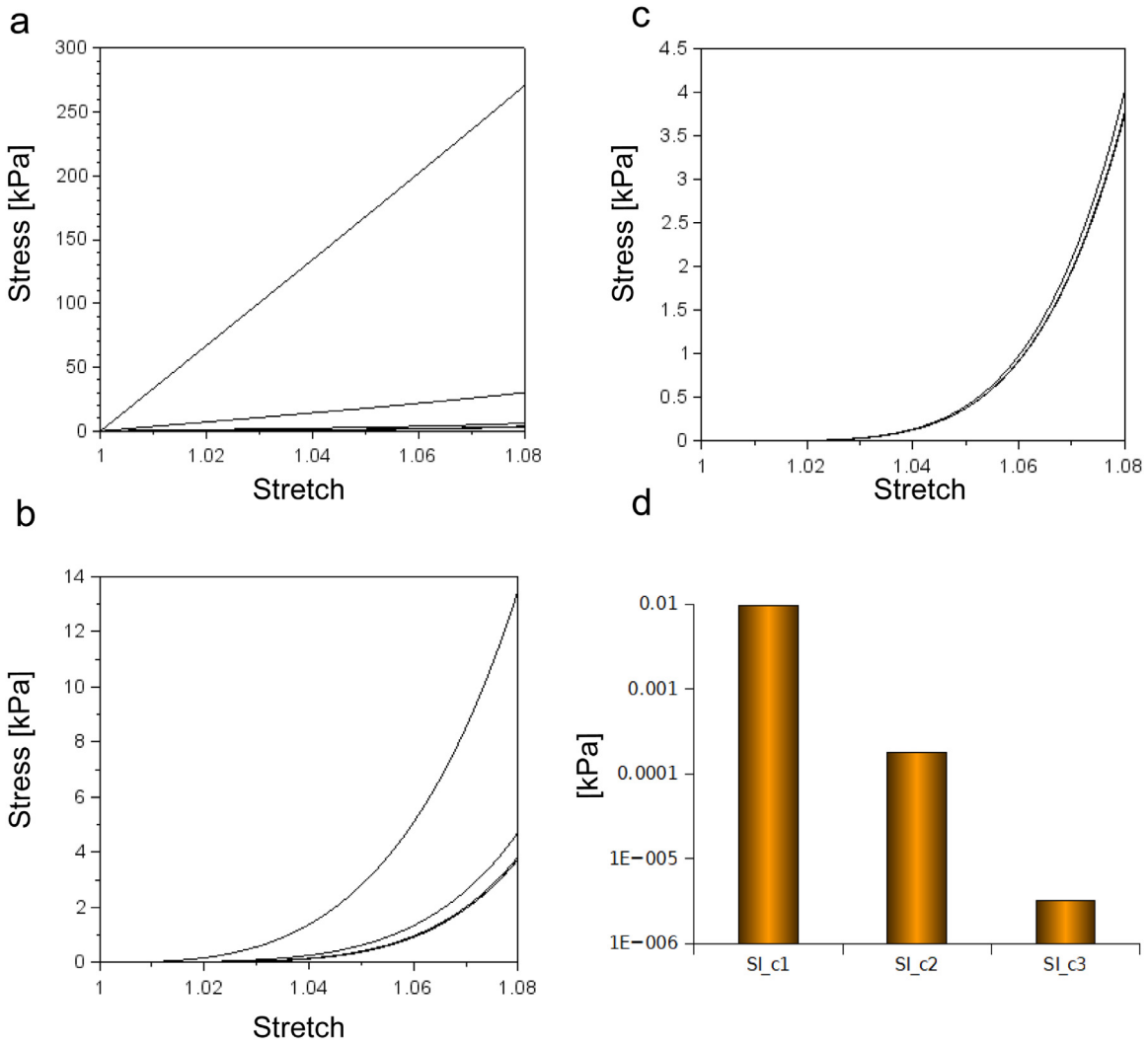

Fig. 3. Tibial nerve. (a) Effect of c_1 variation on the evolution of the theoretical stress curve ($\Delta C_1 = 0.1, 0.5, 1, 10, 100, 1000$). (b) Effect of c_2 variation on the evolution of the theoretical stress curve ($\Delta C_2 = 0.1, 0.5, 1, 10, 100, 1000$). (c) Effect of c_3 variation on the evolution of the theoretical stress curve ($\Delta C_3 = 0.1, 0.5, 1, 10, 100, 1000$). (d) Sensitiveness of the predicted stress with respect to the variation of c_1, c_2, c_3. The values of the sensitiveness index $SI_{c_1} = 1.921 \cdot 10^{-2}$, $SI_{c_2} = 3.544 \cdot 10^{-4}$, $SI_{c_3} = 6.500 \cdot 10^{-6}$ are shown in logarithmic scale.

[17], healthy nerves can, furthermore, progressively increase their instantaneous stiffness. In other words, they show a strain stiffening behaviour, probably to better preserve the integrity of internal axonal fibers. More specifically, even if the non linear evolution of stress as a function of strain (or stretch) is a quite well described phenomenon [31,48], the evolution of the tangent modulus, which is more related to the dynamic change of stiffness, is less studied. Indeed, up to now, a reliable qualitative-quantitative distinction between healthy and pathological response of nerves is lacking. In addition, it is not currently clear whether, when different nerves are stretched, the mean Cauchy stress in their cross section may evolve in a different way.

4.1. Stress-strain evolution

The proposed framework was able to quantitatively reproduce the response of both nerves. Indeed, the mechanical response of specimens was very similar for small strain, as well as at the end of the stretching interval (i.e., $\epsilon = 0.08$). In particular, the mean Cauchy stress in the sciatic nerve exceeded that in the tibial nerve up to $\epsilon = 0.065$, while for further strain it was the opposite. These discrepancies were likely due to the different anatomical location of the two nerves [23], and they were probably related to the minimization of internal stress during physiological strains (e.g., for leg extensions). In addition, the work (for unit of volume) to stretch the tibial nerve specimen up to $\epsilon = 0.08$ was lower than the work required to strain the sciatic nerve specimen. As a consequence, the energetic cost to elongate the tibial nerve was lower for cyclic extension and retraction due to movements. On the contrary, there was a fast increase of stiffness to counteract supra-physiological strain compromising electrical and mechanical functionalities.

4.2. Sensitiveness to parameters

Numerical parameters c_1, c_2, c_3 affected the predicted stress response in a different way. In particular, the influence of the c_1 parameter was about four orders of magnitude greater than the influence of c_3. Similarly, the influence of c_2 was two orders of magnitude greater than the influence of c_3. As a consequence, small changes in c_1 and c_2 affected the final shape of the curve much more than changes in c_3 coefficient. More specifically, c_1 and c_2 were related to the first linear and the following not linear response of nerve, respectively. Thus, changes in c_1 affected the initial "linear elastic" behaviour of the nerve [12], while the following non linear evolution was mainly ruled by the value of c_2. Finally, the value of c_3 affected the non linear evolution of the curve in the

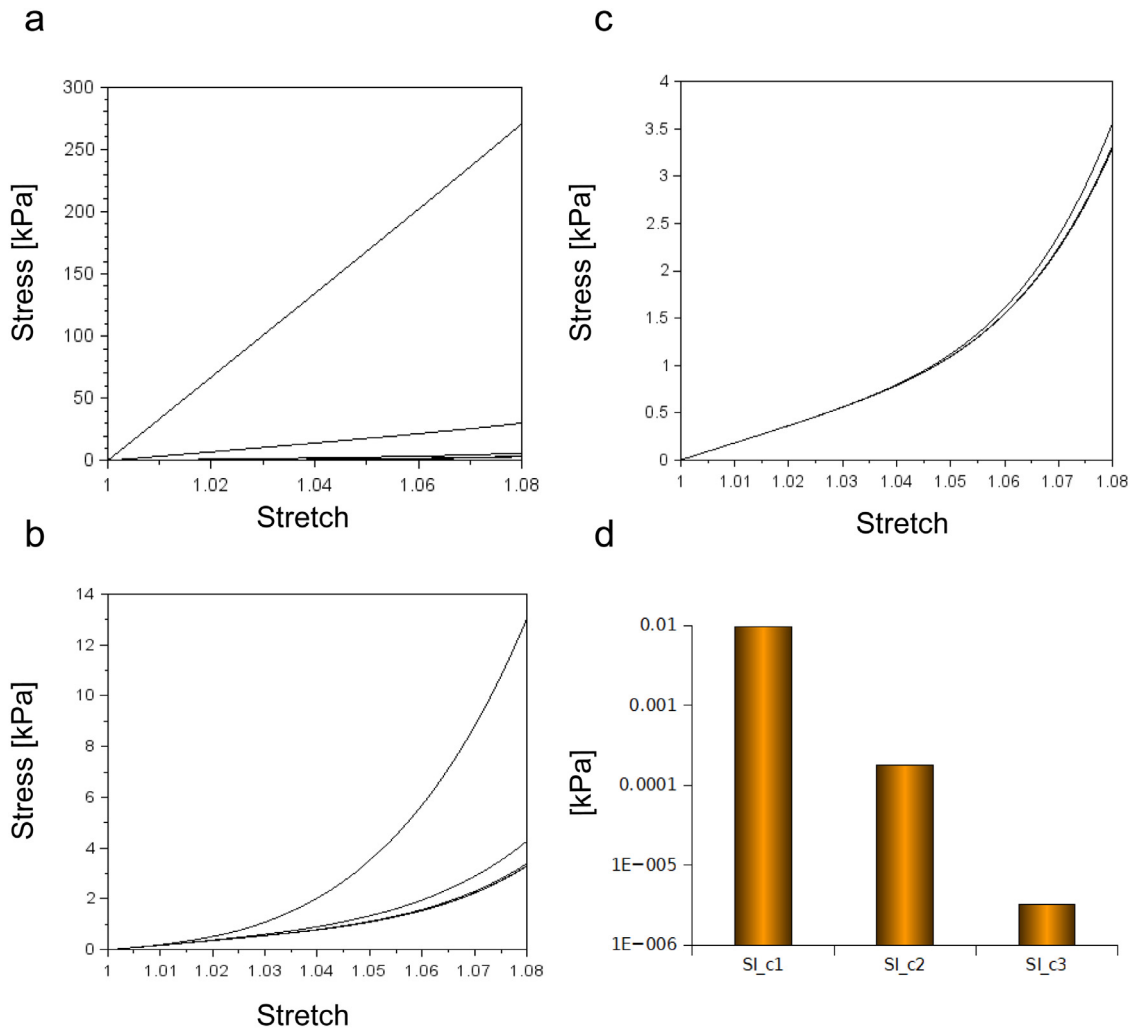

Fig. 4. Sciatic nerve. (a) Effect of c_1 variation on the evolution of the theoretical stress curve ($\Delta C_1 = 0.1, 0.5, 1, 10, 100, 1000$). (b) Effect of c_2 variation on the evolution of the theoretical stress curve ($\Delta C_2 = 0.1, 0.5, 1, 10, 100, 1000$). (c) Effect of c_3 variation on the evolution of the theoretical stress curve ($\Delta C_3 = 0.1, 0.5, 1, 10, 100, 1000$). (d) Sensitiveness of the predicted stress with respect to the variation of c_1, c_2, c_3. The values of the sensitiveness index (SI) $SI_{c_1} = 1.921 \cdot 10^{-2}$, $SI_{c_2} = 3.544 \cdot 10^{-4}$, $SI_{c_3} = 6.500 \cdot 10^{-6}$ are shown in logarithmic scale.

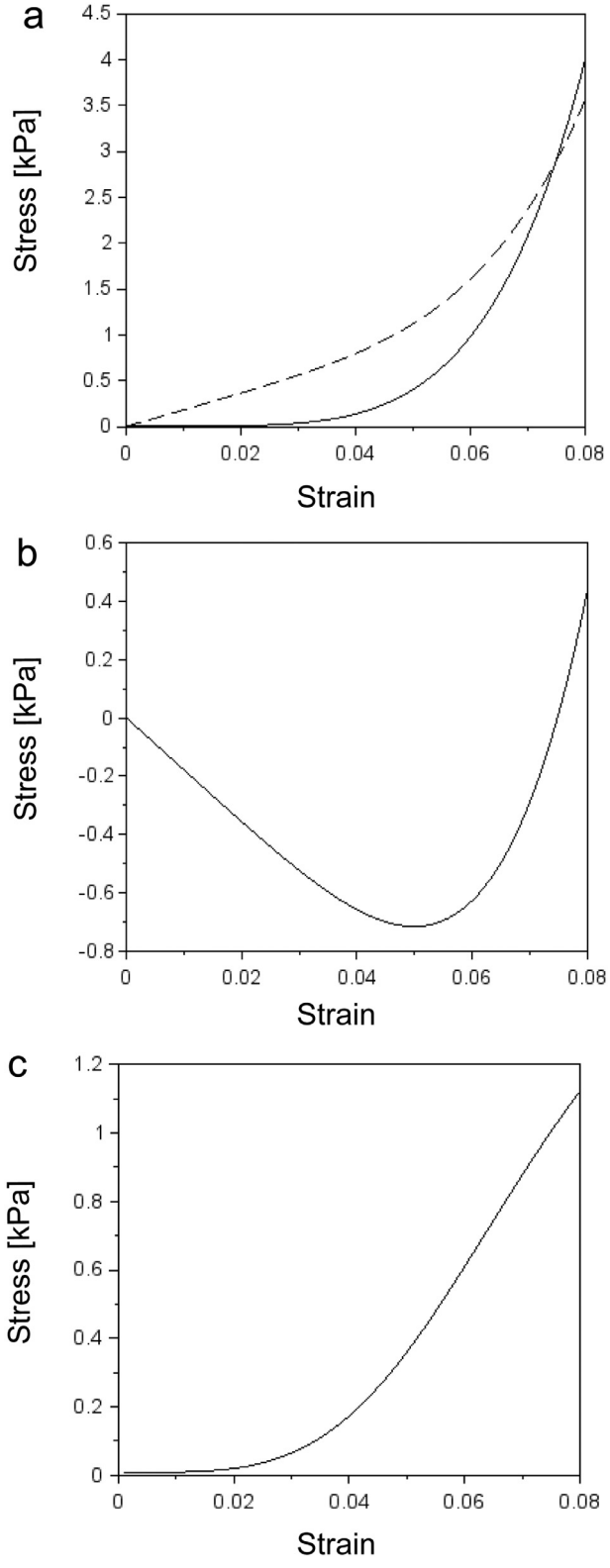

Fig. 5. (a) Evolution of theoretical stress in tibial (solid line) and sciatic nerves (dashed line) ($0 \leq \epsilon \leq 0.08$): initially, the mean Cauchy stress in the tibial nerve specimen was lower than the mean Cauchy stress in the sciatic nerve specimen ($0 \leq \epsilon \leq 0.07$). (b) Evolution of the difference of stress between tibial and sciatic nerves. The maximum difference was close to $\epsilon = 0.05$. (c) Evolution of the ratio between stress in tibial and sciatic nerves. The stress in tibial nerve specimen was initially very low ($\epsilon \simeq 0$), while it exceeded 1.1 times the stress in the sciatic nerve specimen at $\epsilon = 0.08$.

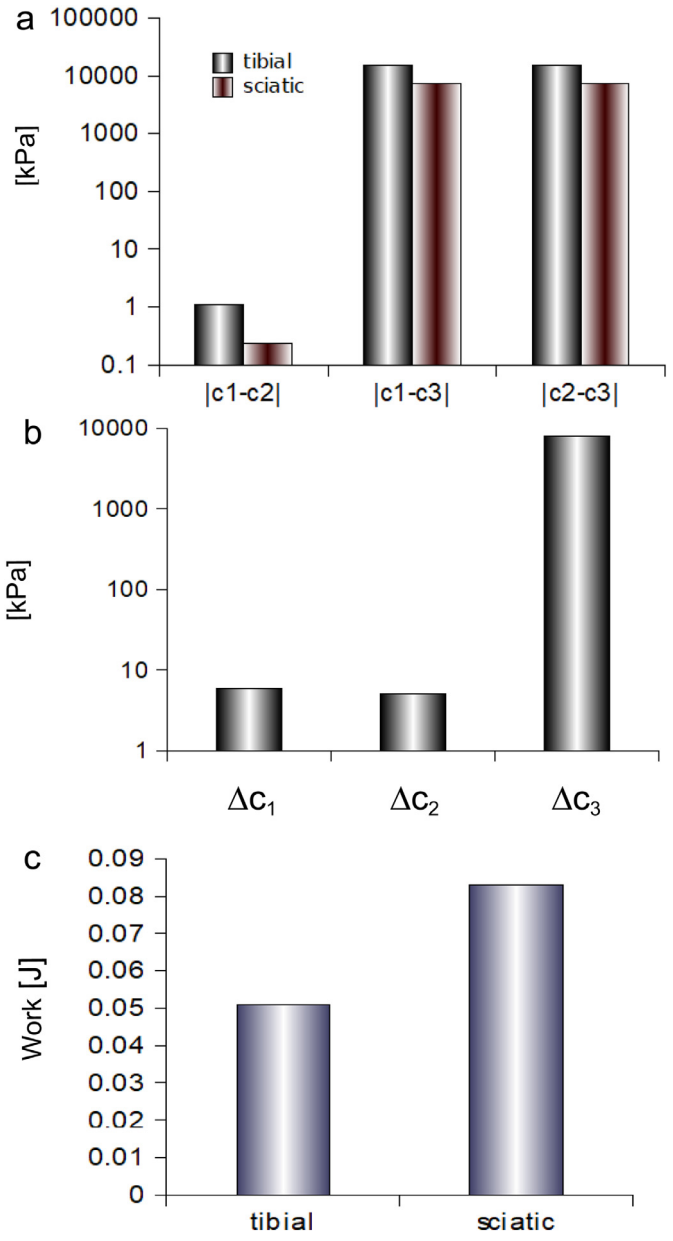

Fig. 6. (a) Difference between coefficients c_1, c_2, c_3 for sciatic and tibial nerve specimens. (b) Difference between values of c_1, c_2, c_3 coefficients in sciatic and tibial nerves. (c) Work for unit of volume to stretch nerves up to $\epsilon = 0.08$.

range $0.06 \leq \epsilon \leq 0.08$, so the sensitiveness of the global curve with respect to this coefficient was low. All these considerations were resumed within the sensitiveness index (SI), since $SI_{c_1} > SI_{c_2} > SI_{c_3}$. This index was also stable with respect to numerical oscillations and, therefore, it was suitable to assess data coming from different specimens.

4.3. Strain stiffening of peripheral nerves: Evolution and variation of tangent modulus

The tangent modulus was used to quantify the nerve ability of changing the instantaneous stiffness. More specifically, the tibial nerve was able to increase its instantaneous stiffness 1571.351 times, while the sciatic nerve was able to harden 7.252 times in the range $0 \leq \epsilon \leq 0.08$.

Furthermore, the sciatic nerve was instantaneously stiffer than the tibial one for $0 \leq \epsilon < 0.05$ (i.e., about 123 times for very small

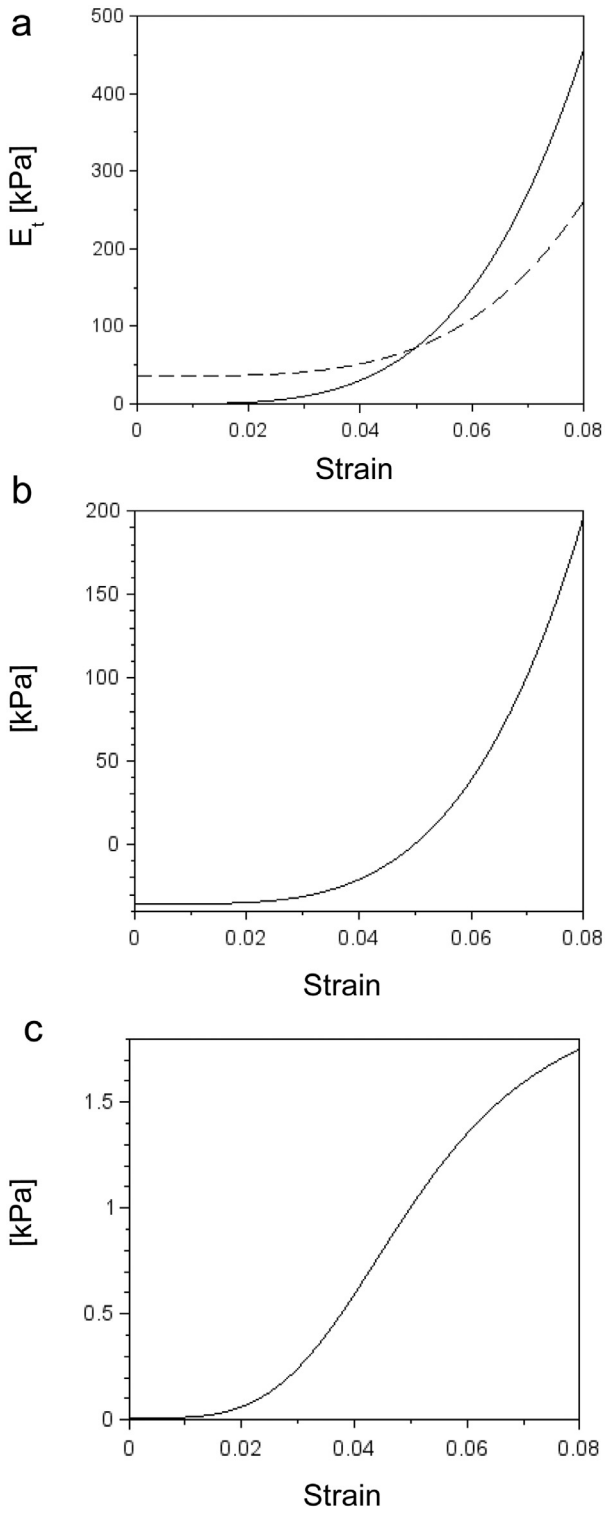

Fig. 7. (a) Evolution of the tangent modulus for tibial (solid line) and sciatic (dashed line) nerve specimens. (b) Evolution of the difference between tangent moduli of tibial and sciatic nerves. (c) Evolution of the ratio between tangent moduli of tibial and sciatic nerves.

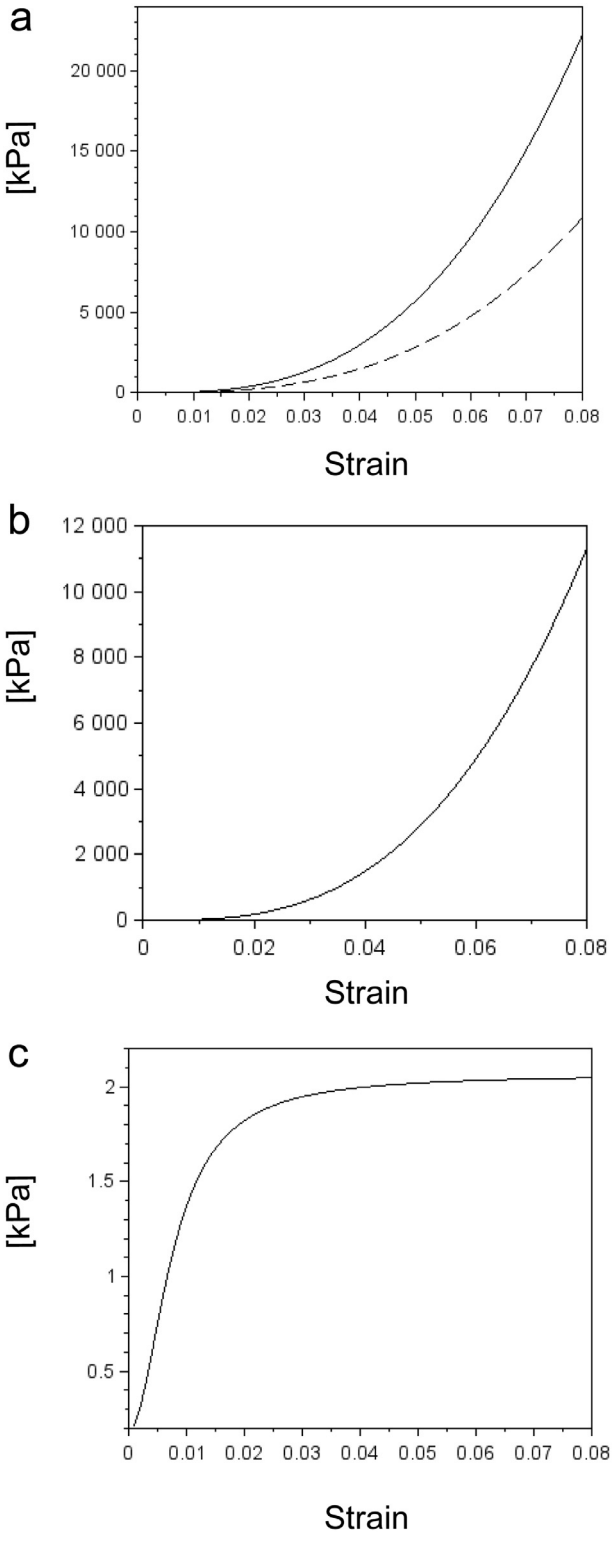

Fig. 8. (a) Evolution of the rate of change of the tangent modulus for tibial (solid line) and sciatic (dashed line) nerve specimens. (b) Difference between the rate of change of the tangent modulus between tibial and sciatic nerve specimens. (c) Ratio between the rate of change of the tangent modulus between tibial and sciatic nerve specimens.

strains), while the change of stiffness was always faster for the tibial nerve in the range $0.05 < \epsilon \leq 0.08$ (i.e., about 1.75 times at $\epsilon = 0.08$). Curiously, both nerves had the same stiffness for mild strain (exactly at $\epsilon = 0.04989766480442918$).

Similarly, the rate of change of the tangent modulus increased from 0 to about 11 MPa [stress/strain^2] and from 0 to about 5.4 MPa [stress/strain^2] for the tibial and the sciatic nerve specimen, respectively. The rate of change of stiffness was always faster for the tibial nerve specimen (i.e.,$0 < \epsilon \leq 0.08$), while the value of the ratio between these rates changed along the strain range. In particular, it firstly increased (i.e., $0 < \epsilon \leq 0.02$), then it deflected (i.e., $0.02 \leq \epsilon \leq 0.03$) and finally it stabilized (i.e.,$0.04 \leq \epsilon \leq 0.08$).

In other words, at low strain, the rate of change of the tibial nerve stiffness was lower than the rate of change of the sciatic nerve stiffness.

On the contrary, for mild strain, the ratio increased and became constant close to $\epsilon = 0.08$. As a consequence, the response of two specimens was progressively similar, even if scaled of a factor $\simeq 2$. In particular, the tibial nerve was more compliant for low strain, while it was able to stiffen more efficiently than the sciatic nerve for high strain (about two times faster).

5. Conclusions

Simple elastic materials keep their stiffness constant with strain before the yielding or rupture point. On the contrary, peripheral nerves under stretch behave in a more complex way, varying their instantaneous stiffness. Therefore, in this work, the evolution of the rate of change of the tangent modulus of peripheral nerves were reproduced through a computational framework able to quantitatively detect changes between different nerves. The analysis was performed over results obtained from two different specimens deriving from and adult pig. As a consequence, more studies are needed to better understand whether, in general, tibial and sciatic nerve behave in a different way when stretched. Nevertheless, the suggested framework was general enough to closely reproduce all experimental data. Indeed, it was able to provide reliable predictions for both specimens, even if stress in tibial and sciatic nerves evolved in a different way. This knowledge could be exploited to provide an early detection of effects due to pathological states related to the nerve stiffness (i.e., neuromalacia) [34], as well as strategic to mimic the behaviour of nerves [31,48] for established medical procedures, as suturing nerve gaps [19,20,47], and for high technological applications. Indeed, novel technological horizons have been opened through the use of neural interfaces [1,15,18,22,24,33,35,44] stretchable electronics [25], as well as through the direct connection between engineered biomaterials and neural cells [5,36,38,41–43] or peripheral nerves [27]. In addition, the last in vivo frontier is related to the challenging control of the immune response of the nerve tissue [2,30,32]. It is currently known that this adverse response is related to the stiffness mismatch between nerve tissue and biomaterials [25]. Nevertheless, this mismatch is likely due not only to a “static” difference (i.e., the actual difference of stiffness at a given strain), but also to the dynamic evolution of stiffness with strain. As a consequence, to design better stretchable electronic devices, both “static” and “dynamic” responses of nerves should be closely approximated to mimic their natural behaviour and to minimize the production of scar tissue. Therefore, the study of the variation and change of the tangent modulus with strain could help in evaluating novel materials [7,46,50,51] to mimic this complex response.

Funding

None.

Ethical approval

Not required.

Declaration of Competing Interest

None declared.

Acknowledgments

The authors thank the company Desideri Luciano s.r.l (approved according to Regulation (EC) 853/2004) for biological specimens, and Dr. Cesare Temporin for his valuable technical assistance in handling and dissection of peripheral nerves.

References

[1] Kotov Nicholas A., Winter Jessica O., Clements Isaac P., Edward J., Timko Brian P., Stéphane C., Smita P., Andrea M., Lieber Charles M., Maurizio P., Bellamkonda Ravi V., Silva Gabriel A., Shi K. N. W., Fernando P., Laura B.. Nanomaterials for neural interfaces. Adv Mater 21(40):3970–4004.. 10.1002/adma.200801984
[2] Anderson JM, Rodriguez A, Chang DT. Foreign body reaction to biomaterials. Semin Immunol 2008;20(2):86–100. doi:10.1016/j.smim.2007.11.004. Innate and Adaptive Immune Responses in Tissue Engineering
[3] Bora FW, Richardson S, Black J. The biomechanical responses to tension in a peripheral nerve. J Hand Surg Am 1980;5(1):21–5. https://doi.org/10.1016/S0363-5023(80)80037-2.
[4] Castro J, Frank P. Stingers, cervical cord neurapraxia, and stenosis. Clin Sports Med 2003;22:483–92.
[5] Ciofani G, Sergi PN, Carpaneto J, Micera S. A hybrid approach for the control of axonal outgrowth: preliminary simulation results. Med Biol Eng Comput 2011;49:163–70. doi:10.1007/s11517-010-0687-x.
[6] Cutrone A, Sergi PN, Bossi S, Micera S. Modelization of a self-opening peripheral neural interface: a feasibility study.. Med Eng Phys 2011;33(10):1254–61. doi:10.1016/j.medengphy.2011.06.001.
[7] Daly W, Yao L, Zeugolis D, Windebank A, Pandit A. A biomaterials approach to peripheral nerve regeneration: bridging the peripheral nerve gap and enhancing functional recovery. J R Soc Interface 2011;9(67):202–21. doi:10.1098/rsif.2011.0438.
[8] DENNY-BROWN D, DOHERTY MM. Effects of transient stretching of peripheral nerve. Arch Neurol Psych 1945;54(2):116–29. doi:10.1001/archneurpsyc.1945.02300080044005.
[9] Dilley A, Lynn B, Greening J, DeLeon N. Quantitative in vivo studies of median nerve sliding in response to wrist, elbow, shoulder and neck movements. Clin Biomech 2003;18(10):899–907. doi:10.1016/S0268-0033(03)00176-1.
[10] Dilley A, Summerhayes C, Lynn B. An in vivo investigation of ulnar nerve sliding during upper limb movements. Clin Biomech 2007;22(7):774–9. doi:10.1016/j.clinbiomech.2007.04.004.
[11] Fung YC. Biomechanics, mechanical properties of living tissues. New York: Springer; 1993.
[12] Giannessi E, Stornelli MR, Coli A, Sergi PN. A quantitative investigation on the peripheral nerve response within the small strain range. App Sci 2019;9(6). doi:10.3390/app9061115.
[13] Giannessi E, Stornelli MR, Sergi PN. A unified approach to model peripheral nerves across different animal species. Peer J 2017;5:e4005. doi:10.7717/peerj.4005.
[14] Giannessi E, Stornelli MR, Sergi PN. Fast in silico assessment of physical stress for peripheral nerves. Med Biol Eng Comput 2018. doi:10.1007/s11517-018-1794-3.
[15] Green RA, Lovell NH, Wallace GG, Poole-Warren LA. Conducting polymers for neural interfaces: challenges in developing an effective long-term implant. Biomaterials 2008;29(2425):3393–9. doi:10.1016/j.biomaterials.2008.04.047.
[16] Greenberg J, Leung D, Kendall J. Predicting chronic stinger syndrome using the mean subaxial space available for the cord index. Sports Health Multidiscipl Approach 2011;3(3):264–7. doi:10.1177/1941738111403866.
[17] Grewal R, Xu J, Sotereanos D, SL W. Biomechanical properties of peripheral nerves.. Hand Clin 1996;12(2):195–204.
[18] Grill WM, Norman SE, Bellamkonda RV. Implanted neural interfaces: biochallenges and engineered solutions.. Annu Rev Biomed Eng 2009;11:1–24. doi:10.1146/annurev-bioeng-061008-124927.
[19] Highet WB, Holmes W. Traction injuries to the lateral popliteal nerve and traction injuries to peripheral nerves after suture. BJS 1943;30(119):212–33. doi:10.1002/bjs.18003011906.
[20] Highet WB, Sanders FK. The effects of stretching nerves after suture. BJS 1943;30(120):355–69. doi:10.1002/bjs.18003012012.
[21] Johnson WD, Storts RW. Peripheral neuropathy associated with dietary riboflavin deficiency in the chicken i. light microscopic study. Vet Pathol 1988;25(1):9–16. doi:10.1177/030098588802500102. PMID: 2830700
[22] Kipke DR, Shain W, Buzsáki G, Fetz E, Henderson JM, Hetke JF, et al. Advanced neurotechnologies for chronic neural interfaces: new horizons and clinical opportunities. J Neurosci 2008;28(46):11830–8. doi:10.1523/JNEUROSCI.3879-08.2008.
[23] Koike H. The extensibility of aplysia nerve and the determination of true axon length.. J Physiol (Lond) 1987;390(1):469–87. doi:10.1113/jphysiol.1987.sp016712.
[24] Kozai TDY, Langhals NB, Patel PR, Deng X, Zhang H, Smith KL, et al. Ultrasmall implantable composite microelectrodes with bioactive surfaces for chronic neural interfaces. Nat Mater 2012;11:1065. doi:10.1038/nmat3468.
[25] Lacour SP, Courtine G, Guck J. Materials and technologies for soft implantable neuroprostheses. Nat Rev Mater 2016;1:16063. doi:10.1038/natrevmats.2016.63.
[26] Lundborg G. Limb ischemia and nerve injury.. Arch Surg 1972;104(5):631–2.
[27] Lundborg G, Gelberman RH, Longo FM, Powell HC, Varon S. In vivo regeneration of cut nerves encased in silicone tubes: growth across a six-millimeter gap.. J Neuropathol Exp Neurol 1982;41(4):412–22.

[28] Ma Z, Hu S, Tan JS, Myer C, Njus NM, Xia Z. In vitro and in vivo mechanical properties of human ulnar and median nerves.. J Biomed Mater Res A 2013;101(9):2718–25. doi:10.1002/jbm.a.34573.
[29] Main EK, Goetz JE, Rudert MJ, Goreham-Voss CM, Brown TD. Apparent transverse compressive material properties of the digital flexor tendons and the median nerve in the carpal tunnel.. J Biomech 2011;44(5):863–8. doi:10.1016/j.jbiomech.2010.12.005.
[30] Malik AF, Hoque R, Ouyang X, Ghani A, Hong E, Khan K, et al. Inflammasome components asc and caspase-1 mediate biomaterial-induced inflammation and foreign body response. Proc Natl Acad Sci 2011;108(50):20095–100. doi:10.1073/pnas.1105152108.
[31] Millesi H, Zoch G, Reihsner R. Mechanical properties of peripheral nerves.. Clin Orthop Relat Res 1995(314):76–83.
[32] Nachemson AK, Lundborg G, Myrhage R, Rank F. Nerve regeneration and pharmacological suppression of the scar reaction at the suture site. an experimental study on the effect of estrogen-progesterone, methylprednisolone-acetate and cis-hydroxyproline in rat sciatic nerve.. Scand J Plast Reconstr Surg 1985;19(3):255–60.
[33] Navarro X, Krueger TB, Lago N, Micera S, Stieglitz T, Dario P. A critical review of interfaces with the peripheral nervous system for the control of neuroprostheses and hybrid bionic systems.. J Peripher Nerv Syst 2005;10(3):229–58. doi:10.1111/j.1085-9489.2005.10303.x.
[34] Nonaka Y, Fukushima T, Watanabe K, Friedman AH, Cunningham CD, Zomorodi AR. Surgical management of vestibular schwannomas after failed radiation treatment. Neurosurg Rev 2016;39(2):303–12. doi:10.1007/s10143-015-0690-7.
[35] Reza AM, MD C. Multifunctional nanobiomaterials for neural interfaces. Adv Funct Mater 2009;19(4):573–85. doi:10.1002/adfm.200801473.
[36] Roccasalvo IM, Micera S, Sergi PN. A hybrid computational model to predict chemotactic guidance of growth cones. Sci Rep 2015;5. doi:10.1038/srep11340. 11340
[37] Sergi PN, Carrozza MC, Dario P, Micera S. Biomechanical characterization of needle piercing into peripheral nervous tissue.. IEEE Trans Biomed Eng 2006;53(11):2373–86. doi:10.1109/TBME.2006.879463.
[38] Sergi PN, Cavalcanti-Adam EA. Biomaterials and computation: a strategic alliance to investigate emergent responses of neural cells. Biomater Sci 2017;5:648–57. doi:10.1039/C6BM00871B.
[39] Sergi PN, Jensen W, Micera S, Yoshida K. In vivo interactions between tungsten microneedles and peripheral nerves.. Med Eng Phys 2012;34(6):747–55. doi:10.1016/j.medengphy.2011.09.019.
[40] Sergi PN, Jensen W, Yoshida K. Interactions among biotic and abiotic factors affect the reliability of tungsten microneedles puncturing in vitro and in vivo peripheral nerves: a hybrid computational approach. Mater Sci Eng C 2016;59:1089–99. doi:10.1016/j.msec.2015.11.022.
[41] Sergi PN, Marino A, Ciofani G. Deterministic control of mean alignment and elongation of neuron-like cells by grating geometry: a computational approach. Integr Biol 2015;7:1242–52. doi:10.1039/C5IB00045A.
[42] Sergi PN, Morana Roccasalvo I, Tonazzini I, Cecchini M, Micera S. Cell guidance on nanogratings: a computational model of the interplay between pc12 growth cones and nanostructures. PLoS ONE 2013;8(8):e70304. doi:10.1371/journal.pone.0070304.
[43] Spira ME, Hai A. Multi-electrode array technologies for neuroscience and cardiology. Nat Nanotechnol 2013;8:83. doi:10.1038/nnano.2012.265.
[44] Stieglitz T, Beutel H, Schuettler M, Meyer J-U. Micromachined, polyimide-based devices for flexible neural interfaces. Biomed Microdev 2000;2(4):283–94. doi:10.1023/A:1009955222114.
[45] Sunderland S. The intraneural topography of the radial, median and ulnar nerves.. Brain 1945;68:243–99.
[46] Tao J, Hu Y, Wang S, Zhang J, Liu X, Gou Z, et al. A 3d-engineered porous conduit for peripheral nerve repair. Sci Rep 2017;7:46038. doi:10.1038/srep46038.
[47] Terzis J, Faibisoff B, Williams B. The nerve gap: suture under tension vs. graft.. Plast Reconstr Surg 1975;56(2):212–33.
[48] Topp KS, Boyd BS. Structure and biomechanics of peripheral nerves: nerve responses to physical stresses and implications for physical therapist practice.. Phys Ther 2006;86(1):92–109.
[49] Vogl AW, Lillie MA, Piscitelli MA, Goldbogen JA, Pyenson ND, Shadwick RE. Stretchy nerves are an essential component of the extreme feeding mechanism of rorqual whales. Curr Biol 2015;25(9):R360–1. doi:10.1016/j.cub.2015.03.007.
[50] Wang S, Yaszemski MJ, Knight AM, Gruetzmacher JA, Windebank AJ, Lu L. Photo-crosslinked poly(ϵ-caprolactone fumarate) networks for peripheral nerve regeneration: physical properties and preliminary biological evaluations. Acta Biomater 2009;5(5):1531–42.
[51] Wang Y, Ameer GA, Sheppard BJ, Langer R. A tough biodegradable elastomer. Nat Biotechnol 2002;20:602. doi:10.1038/nbt0602-602.
[52] Williams MJ, Utzinger U, Barkmeier-Kraemer JM, Vande Geest JP. Differences in the microstructure and biomechanical properties of the recurrent laryngeal nerve as a function of age and location. J Biomech Eng 2014;136(8):0810081–9.
[53] Yeoh OH. Some forms of the strain energy function for rubber. Rubber Chem Technol 1993;66(5):754–71. doi:10.5254/1.3538343.
[54] Yoshida K, Lewinsky I, Nielsen M, Hylleberg M. Implantation mechanics of tungsten microneedles into peripheral nerve trunks.. Med Biol Eng Comput 2007;45(4):413–20. doi:10.1007/s11517-007-0175-0.